Supplementary Information

Untangling the Potential of Non-Entangled Bottlebrush Block Copolymers as Separator Coating Materials for High-Rate and Long-Life Sodium Metal Batteries

Daun Jeong,[ab] Gyu Hwang Shin,[c] Hyojun Lim,[a] Seunghyeon Kim,[d] Da-Sol Kwon,[ae] Jinsol Yook,[f] Sang-Ok Kim,[ag] Kyung Yoon Chung,[ag] Kyeounghak Kim,[c*] and Jimin Shim[d*]

[a] Energy Storage Research Center, Korea Institute of Science and Technology (KIST), 14 Gil 5 Hwarang-ro, Seongbuk-gu, Seoul 02792, Republic of Korea

[b] Department of Chemical Engineering and Materials Science, University of Minnesota, Minneapolis, Minnesota 55455, United States

[c] Department of Chemical Engineering, Hanyang University, 222 Wangsimni-ro, Seongdong-gu, Seoul 04763, Republic of Korea

[d] Department of Chemistry Education, Seoul National University, 1 Gwanak-ro, Gwanak-gu, Seoul 08826, Republic of Korea

[e] Department of Chemical and Biological Engineering, Korea University, 145 Anam-ro, Seongbuk-gu, Seoul 02841, Republic of Korea

[f] Department of Chemistry, University of Minnesota, Minneapolis, Minnesota 55455, United States

[g] Division of Energy & Environment Technology, KIST School, University of Science and Technology, Seoul 02792, Republic of Korea

* E-mail: chemekim@hanyang.ac.kr (K. Kim) and jiminshim@snu.ac.kr (J. Shim)

Experimental method

Materials. *cis*–5–norbornene–*endo*–2,3–dicarboxylic anhydride, ethanolamine, triethylamine (TEA), 2-bromo-2-methylpropionyl bromide (BIBB), poly(ethylene glycol) methyl ether methacrylate (PEGMA, average M_n: 300 g mol^{-1}), glycidyl methacrylate (GMA), styrene, copper bromide (CuBr), *N,N,N′,N″,N″*-pentamethyldiethylenetriamine (PMDETA), Grubbs Catalyst® 3rd Generation (G3, M300), ethyl vinyl ether, and sodium trifluoromethanesulfonate (NaTFSI) were purchased from Sigma-Aldrich. 1 M sodium hexafluorophosphate ($NaPF_6$) in a mixture of ethylene carbonate (EC), propylene carbonate (PC), and diethyl carbonate (DEC) (1:1:1 vol%) with 2 wt% of fluoroethylene carbonate (FEC) was purchased from Welcos Co., Ltd (Korea). Glass fiber (GF/F, Whatman, thickness: 260 μm) was used as a separator for electrochemical analyses. All other chemicals and solvents were purchased from reliable commercial sources and used as received.

Preparation of *cis*-5-norbornene-*exo*-2,3-dicarboxylic anhydride (NA). NA was prepared by thermally-induced isomerization of *cis*–5–norbornene–*endo*–2,3–dicarboxylic anhydride, as described in our recent publication.[1] ^{1}H NMR (400 MHz, $CDCl_3$): δ [ppm] = 6.34 (C*H*=C*H*, 2H), 3.46 (CH-C*H*-CH, 2H), 3.01 (CO-C*H*, 2H), 1.67 and 1.45 (CH-CH_2-CH, 2H).

Synthesis of *N*-(2-hydroxyethyl)-*cis*-5-norbornene-*exo*-dicarboximide (NI-OH). After dissolving NA (2.00 g, 12 mmol) in toluene (20 mL) at 110 °C, ethanolamine (0.82 g, 13 mmol) and TEA (0.12 g, 1.2 mmol) were added to the solution, and the resultant solution was stirred at 110 °C for 24 h with a reflux condenser. After the reaction, toluene was removed by a rotary evaporator, and the crude solution was diluted with methylene chloride (MC) and extracted

three times: once with 100 mL of 2% (v/v) HCl and twice with 100 mL of brine solution. The organic layer was dried over anhydrous magnesium sulfate and filtered. After drying under vacuum at room temperature, NI-OH was obtained as a white solid. ^{1}H NMR (400 MHz, $CDCl_3$): δ [ppm] = 6.30 (C*H*=C*H*, 2H), 3.78 and 3.72 (N-CH_2-CH_2-OH, 4H), 3.30 (CH-C*H*-CH, 2H), 2.73 (CO-C*H*, 2H), 2.15 (CH_2-O*H*) 1.52 and 1.37 (CH-CH_2-CH, 2H).

Synthesis of *N*-(2-bromopropanoylethyl)-*exo,cis*-2,3-dicarboximide (NI-Br). TEA (0.95 g, 9.4 mmol) and BIBB (2.2 g, 9.4 mmol) were added to the solution of NI-OH (1.3 g, 6.3 mmol) in anhydrous MC (60 mL) at 0 °C, and the resultant solution was stirred at room temperature for 24 h. After the reaction, the crude solution was extracted three times with brine solution. The organic layer was dried over anhydrous magnesium sulfate and filtered. The resultant yellow oil was further purified by column chromatography using silica and hexane/ethylene acetate (1:2 vol%) cosolvent as an eluent. After drying under vacuum at room temperature, NI-Br was obtained as a white powder with a 50% yield. ^{1}H NMR (400 MHz, $CDCl_3$): δ [ppm] = 6.29 (C*H*=C*H*, 2H), 4.34 and 3.82 (N-CH_2-CH_2-OH, 4H), 3.28 (CH-C*H*-CH, 2H), 2.71 (CO-C*H*, 2H), 1.90 (CO-C-(CH_3)$_2$-Br), 1.52 and 1.33 (CH-CH_2-CH, 2H).

Synthesis of poly(PEGMA-*co*-GMA) macromonomer (PPG). A solution of NI-Br (0.32 g, 0.89 mmol), PEGMA (5.0 g, 17 mmol), GMA (0.16 g, 1.1 mmol), and CuBr (0.13 g, 0.89 mmol) in dimethylformamide (DMF, 10 mL) was deoxygenated by three times of freeze-pump-thaw cycles. PMDETA (0.31 g, 1.8 mmol) was then added to the solution, and further deoxygenated by two times of freeze-pump-thaw cycles. The resultant solution was stirred at 70 °C for 10 min. After the reaction, the crude product was diluted by chloroform, passed through a basic alumina column to remove the copper catalyst, and precipitated in hexane five

times. After drying under vacuum at room temperature, PPG was obtained as transparent yellowish wax with a 85% yield.

Synthesis of polystyrene macromonomer (PSt). A mixture of NI-Br (0.086 g, 0.24 mmol), styrene (5.0 g, 48 mmol), and CuBr (0.034 g, 0.24 mmol) in DMF (5.0 mL) was deoxygenated by three times freeze-pump-thaw cycles. After that, PMDETA (0.083 g, 0.48 mmol) was added to the mixture, and the solution was further deoxygenated by two times of freeze-pump-thaw cycles. The resultant solution was stirred at 90 °C for 3.5 h. After the reaction, the crude product was diluted by chloroform and passed through a basic alumina column to remove the copper catalyst, and precipitated in methanol three times for further purification. After drying under vacuum at room temperature, PSt was obtained as a white powder with a 90% yield.

Synthesis of polymerized PPG (Poly(PPG)). PPG (0.2 g) was dissolved in MC (0.8 mL) and a predetermined amount of G3 stock solution was added to the solution ($[M]_0/[G]_0$=46). The resultant solution was stirred at 30 °C for 2 h. After the reaction, the solution was quenched with 0.1 mL of ethyl vinyl ether, and the crude solution was precipitated in diethyl ether three times. After drying under vacuum, poly(PPG) corresponding to the first block of the bottlebrush block copolymer was obtained as a viscous wax with an 81% yield.

Synthesis of poly(PPG-*b*-PSt) bottlebrush block copolymer (BBP). PPG (1.0 g) was dissolved in MC (4.2 mL) and a predetermined amount of G3 stock solution was added to the solution ($[M]_0/[G]_0$=55). The resultant solution was stirred at 30 °C for 2 h, and the PSt solution in MC (0.67 mL, 0.050 M) was added. After 2 h, the reaction was quenched with 0.1 mL of

ethyl vinyl ether. The crude solution was precipitated in diethyl ether three times. After drying under vacuum, BBP was obtained as a sticky solid with a 90% yield.

Preparation of GF coated with NaTFSI-doped BBP (GF-NaBBP). GF was immersed in a solution of BBP (0.080 g) and NaTFSI (0.036 g, $[Na^+]/[EO]=0.13$) in anhydrous tetrahydrofuran (THF, 1.0 mL) for 2 h. Subsequently, it was dried under vacuum at 30 °C for 3 h and further at 120 °C for 15 h to react the epoxy group of GMA with the hydroxyl group of the GF membrane. The resulting GF-NaBBP was slowly cooled in a vacuum oven to induce phase separation.

Synthesis of Prussian blue analogue (PBA, $Na_{2-x}Fe[Fe(CN)_6]$). PBA was synthesized by the previously reported precipitation method.[2] A solution of trisodium citrate (7.50 g) and $FeSO_4 \cdot 7H_2O$ (1.67 g) in deionized (DI) water (100 mL) was prepared by stirring at room temperature under N_2 bubbling. The prepared solution was added dropwise to the solution of trisodium citrate (7.50 g) and $Na_4Fe(CN)_6 \cdot 10H_2O$ (1.96 g) in DI water (100 mL) while stirring, and the resultant solution was stirred at 800 rpm for 6 h under N_2 condition. The final product was collected by centrifugation and washed with DI water several times. After drying overnight under a dynamic vacuum at 120 °C, PBA was obtained as a black powder.

Preparation of PBA cathode. PBA (70 wt%) was used as a cathode active material and dispersed in NMP with Super P (20 wt%) and PVDF binder (Solef 6020) (10 wt%) using a Thinky mixer. The resultant slurry was uniformly cast onto an aluminum (Al) current collector using a doctor blade, followed by drying under vacuum at 80 °C to remove the residual NMP.

The mass loading of the active materials in the cathode was approximately in the range of 3–4 mg cm^{-2}.

Electrochemical Characterizations. The liquid electrolyte uptake was determined by measuring the changes in weight before and after immersion in 1 M $NaPF_6$ in EC:PC:DEC (1:1:1 vol%) with 2 wt% of FEC for 24 h. The resulting electrolyte uptake value was determined by the following equation (1):

$$\text{Electrolyte uptake (\%)} = (W_{wet} - W_{dry})/W_{dry} \times 100 \quad (1)$$

where W_{dry} and W_{wet} are the weights before and after immersion in liquid electrolytes, respectively. The electrolyte-wetted GF and GF-NaBBP separators were prepared by immersing in 1 M $NaPF_6$ in EC:PC:DEC (1:1:1 vol%) with 2 wt% of FEC for 24 h in an argon-filled glove box (O_2 < 0.1 ppm, H_2O < 0.1 ppm) prior to the electrochemical analyses. Ionic conductivities were determined by AC impedance spectroscopy using a VMP3 multi-channel potentiostat (Biologic, France) in a frequency range from 10 Hz to 1 MHz with a 10 mV amplitude at 30 °C. The samples were prepared by sandwiching the separators between two stainless-steel electrodes in a 2032-coin cell. The ionic conductivity (σ) was determined by the following equation (2):

$$\sigma = (1/R) \times (d/A) \quad (2)$$

where R is the resistance obtained from the impedance spectrum, d is the thickness of the membrane, and A is the area of the electrode. Linear sweep voltammetry (LSV) was performed using a VMP3 multi-channel potentiostat (Biologic, France) in a voltage range of 3.0–7.0 V (*vs*. Na/Na^+) at a scan rate of 1.0 mV s^{-1}. Cyclic voltammetry (CV) was performed using a VMP3 multi-channel potentiostat (Biologic, France) in a voltage range of 2.0–4.5 V (*vs*.

Na/Na^+) at a scan rate of 1.0 mV s^{-1}. Charge/discharge cycling test of Na/separator/PBA cell was conducted at a cut-off voltage range of 2.0–4.0 V (*vs*. Na/Na^+) at 30 °C, where 1 C corresponds to a current density of 120 mA g^{-1}. 1 M $NaPF_6$ in EC:PC:DEC (1:1:1 vol%) with 2 wt% FEC was used as a liquid electrolyte. The galvanostatic cycling test of Na/Na and Na/Cu cells was performed on a WBCS–3000 battery cycle system (WonATech Co., Korea) with a current density of 0.5 mA cm^{-2} and a total capacity of 0.5 mAh cm^{-2} at 30 °C. Electrochemical impedance spectroscopy (EIS) was conducted on a VMP3 multi-channel potentiostat (Biologic, France) in a frequency range from 0.1 to 100 MHz with 10 mV of amplitude at 30 °C. All the cell components were assembled in an argon-filled glove box (O_2 < 0.1 ppm, H_2O < 0.1 ppm).

Instrumentation and characterization techniques. ^{1}H NMR spectra were recorded on an Ascend™ 400 spectrometer (400 MHz) using $CDCl_3$ with tetramethylsilane (TMS) reference (Sigma-Aldrich) as a solvent at room temperature. Molar mass and dispersity (*Đ*) were determined by size exclusive chromatography (SEC) using the Ultimate 3000 HPLC system (Thermo Fisher Scientific Inc., USA). HPLC grade THF (J. T. Baker®) was used as an eluent. The glass transition temperatures of the polymers were evaluated by differential scanning calorimetry (DSC) using TA Instruments DSC25 under a nitrogen atmosphere (cooling rate: 1 °C min^{-1}, heating rate: 10 °C min^{-1}). Small-angle and wide-angle X-ray scattering (SAXS and WAXS) experiments were performed on SAXS Xeuss 2.0 apparatus (Xenocs) and D8 Discover (Bruker), respectively, at room temperature. A Discovery Hybrid Rheometer (NFEC-2024-09-299197, TA Instruments, USA) equipped with an 8 mm parallel plate geometry was used to determine the linear viscoelastic response of polymers. The specimens were heated and cooled at a rate of 1 °C min^{-1} while monitoring the dynamic storage and loss moduli (G' and G'') at a fixed frequency of 1 rad s^{-1} within the specific temperature range. All the measurements were performed in a linear viscoelastic regime determined by dynamic strain sweep experiments. A

strain amplitude of 1% was employed unless otherwise indicated. Time-temperature superposition (TTS) master curves were constructed by shifting data along the frequency axis at a reference temperature of 110 °C. The nano-indentation test was performed using a TI950 Triboindenter (Hysitron, USA) with a displacement control of 500 nm. Porosity and pore diameter were determined using an AutoPore IV 9500 mercury (Hg) intrusion porosimeter (Micromeritics, USA). Thermogravimetric analysis (TGA) was performed using TA Instruments TGA55 under a nitrogen atmosphere (heating rate: 10 °C min^{-1}). FT-IR spectra were recorded in the absorption mode on the Nicolet 6700 spectrophotometer with a resolution of 8 cm^{-1} in the vibrational frequency range from 400 to 4000 cm^{-1}. 3D X-ray microscopy (XRM) was performed using a Xradia 620 Versa with a spatial resolution of 0.6 μm. X-ray photoelectron spectroscopy (XPS) was performed using a PHI 5000 VersaProbe (ULVAC PHI, Japan) with a monochromatized Al Kα as a radiation source. A survey spectrum was collected over a range of 0–1400 eV, followed by high-resolution narrow scans of C1*s*, O1*s*, F1*s*, Li1*s*, and Ni2*p* regions. Depth profiles were collected using an Ar^+ sputter source with a sputter rate of 0.5 nm s^{-1}. X-ray diffraction (XRD) patterns were recorded using a MiniFlex II (Rigaku, Japan) with a scan speed of 4° min^{-1} in the 2θ range of 10–60°. Scanning electron microscopy (SEM) was performed on a Regulus 8230–Oxford EDS (Hitachi Inc., Tokyo, Japan) at an accelerating voltage of 10 kV. SEM specimens were prepared by washing with dimethyl carbonate (DMC) followed by vacuum drying at room temperature in an argon-filled glove box. A focused ion beam (FIB; Helios NanoLab600, FEI, US) was used to prepare transmission electron microscopy (TEM) samples. The TEM was performed on a Titan TM 80-300 (FEI, Netherlands). Time-of-flight secondary ion mass spectrometry (TOF-SIMS) was performed using a TOFSIMS.5 (ION-TOF, Germany) with a raster size of 50 × 50 μm^2. A Bi^+ beam (30 keV, 1 pA) was used to analyze the depth profile and a Cs^+ beam (3 keV, 20 nA) was used to sputter the electrodes with a sputtering rate of 0.5 nm s^{-1}.

Computational details. Molecular dynamic (MD) simulations were performed using the Materials Studio 2024. In this study, the geometry optimization of all monomers in norbornene-based copolymers was carried out using the Forcite module with Smart algorithm. The convergence tolerances were meticulously set to ensure high precision: energy convergence at 2.0×10^{-5} kcal mol^{-1}, force convergence at 0.001 kcal mol^{-1} Å^{-1}, and displacement convergence at 1.0×10^{-5} Å. To accurately account for non-bonded interactions, atom-based summation method was applied with an electrostatic and van der Waals cutoff distance of 18.5 Å.

The most stable backbone angle of the norbornene-based copolymer was determined using the Conformer module. This method was essential to prevent overlapping between atoms or monomers. To achieve this, a systematic grid scan search method was employed. The analysis focused specifically on the bonds connecting norbornene imide to other monomers and the bonds connecting side chains. These bonds were systematically rotated from –180° to 180° in 30° increments. This approach ensured a comprehensive exploration of possible conformations, thereby identifying the most stable geometric configuration. After the geometric optimization of each monomer, they were built into copolymers and subjected to further geometric optimization using the Forcite module. We conducted simulations for two distinct systems: one for BBP alone, and another for the BBP system with Na^+ ions (NaBBP). All simulations were performed by using the COMPASSIII force field.[3] Van der Waals interactions were handled using the atom-based summation method with a cutoff distance of 15 Å. Long-range electrostatic interactions were managed using the Ewald summation method,[4] with an accuracy of 10×10^{-4} kcal mol^{-1}.

The initial structural modeling of BBP, consisting of 46,277 atoms (C15815 H25192 N55 O5215), was performed using the Amorphous Cell module. Then, the simulations were carried out at room temperature (298 K) over 5000 loading steps. For NaBBP, Na^+ ions were packed into the polymer within the simulation box. Both systems were allowed to reach equilibrium

over a total simulation time of 4.0 ns using the NPT ensemble. Due to the large size of the BBP model, the first 100 ps simulation was conducted with a time step of 0.1 fs to gradually bring the system to equilibrium at 298 K and 1.0 atm. The Nosé-Hoover thermostat and Andersen barostat were used to control the temperature and pressure, respectively.

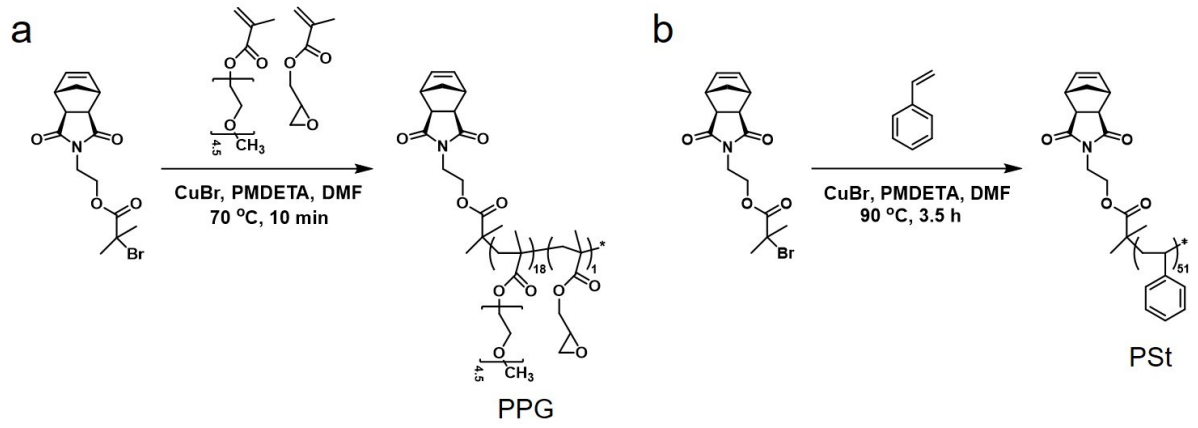

Scheme S1. Synthetic route to a) PPG and b) PSt macromonomers.

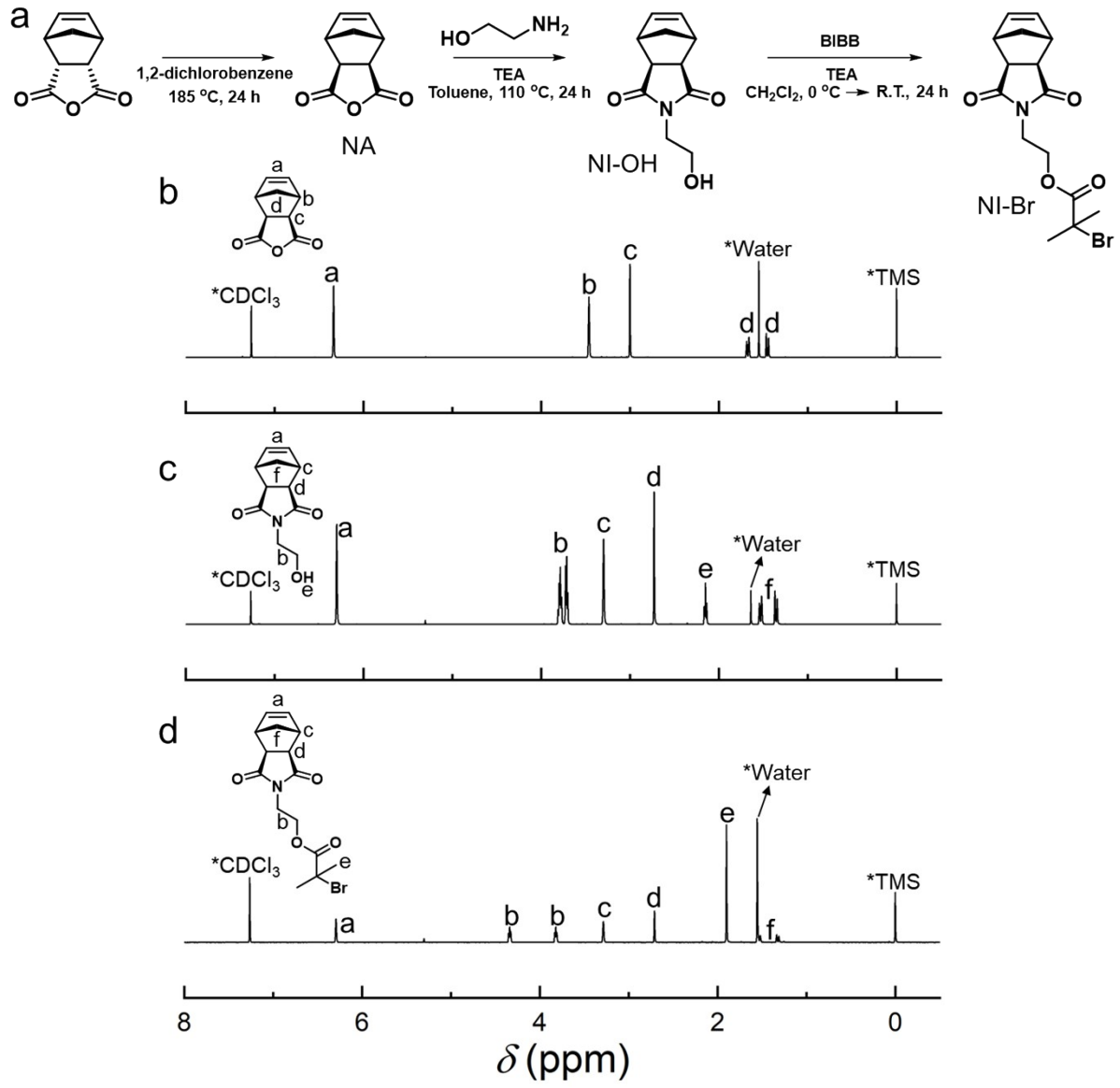

Fig. S1. a) Synthetic route to *N*-(2-bromopropanoylethyl)-*exo,cis*-2,3-dicarboximide (NI-Br). ^{1}H NMR spectrum of b) *cis*-5-norbornene-*exo*-2,3-dicarboxylic anhydride (NA), c) *N*-(2-hydroxyethyl)-*cis*-5-norbornene-*exo*-dicarboximide (NI-OH), and d) NI-Br.

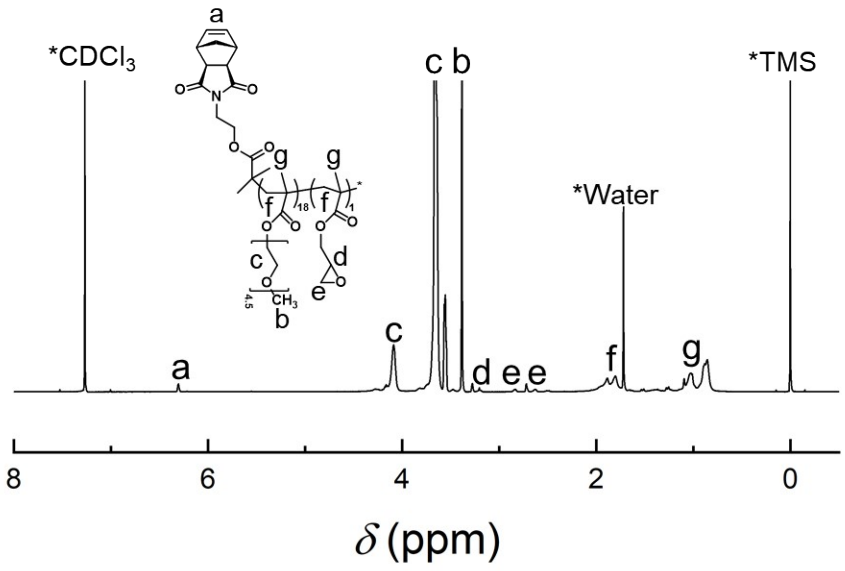

Fig. S2. ^{1}H NMR spectrum of PPG.

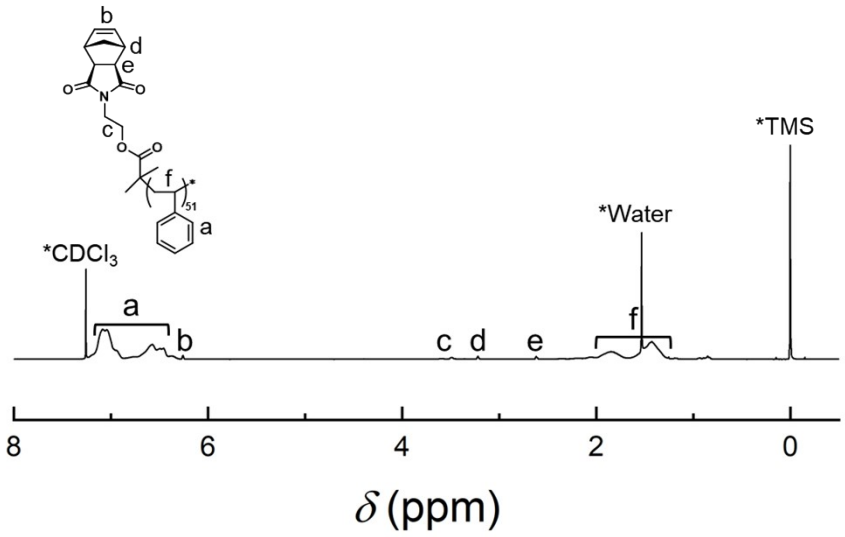

Fig. S3. ^{1}H NMR spectrum of PSt.

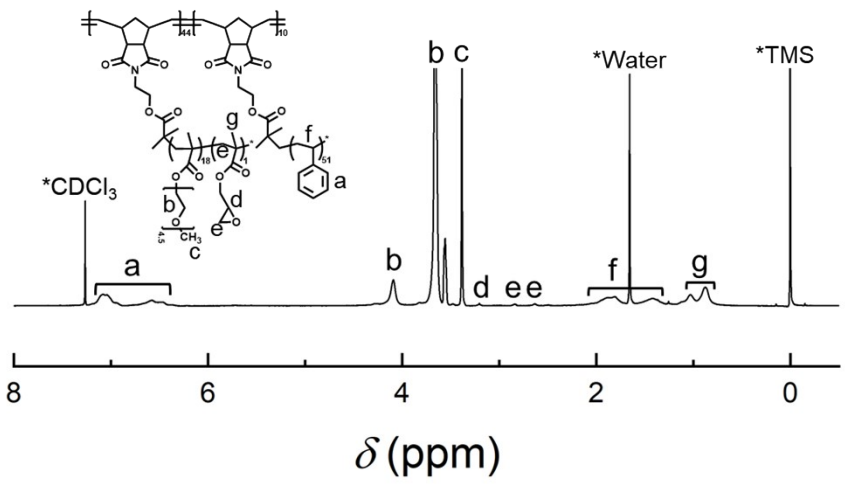

Fig. S4. ^{1}H NMR spectrum of BBP.

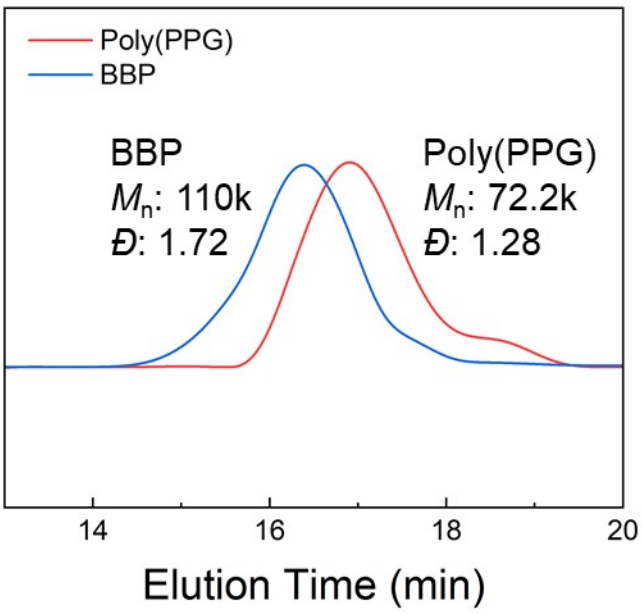

Fig. S5. SEC chromatograms of poly(PPG) and BBP (eluent: THF).

Table S1. Molecular characteristics of PPG, PSt, and BBP.

Polymer	M_n (kDa)[a]	$Đ$[b]	f_{PPG}[c]	N_{sc}[d]	N_{bb}[e]
PPG	5.95	1.12	-	18.1	-
PSt	5.70	1.11	-	51.3	-
BBP	322	1.72	0.82	-	54.5

[a]Number-average molecular weights determined by ^{1}H NMR spectroscopy. [b]Dispersities obtained by SEC in THF as the eluent. [c]Volume fraction of PPG block determined by ^{1}H NMR spectroscopy. Number-average degree of polymerization of [d]PPG and PSt side chains and [e]BBP backbone, where sc and bb indicate side chain and backbone, respectively.

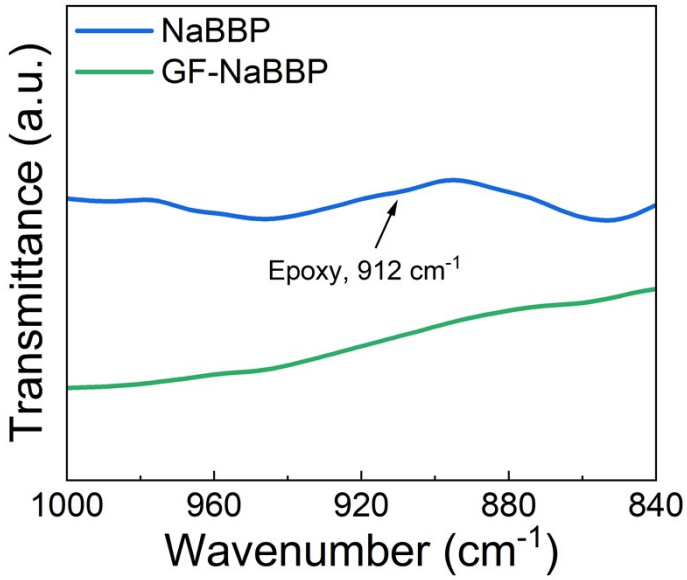

Fig. S6. FT-IR spectra of NaBBP and GF-NaBBP.

The disappearance of the epoxy peak at 912 cm^{-1} after the heat treatment of GF-NaBBP at 120 ºC confirms the cross-linking reaction between the glycidyl moieties of BBP and the surface hydroxyl groups of GF.

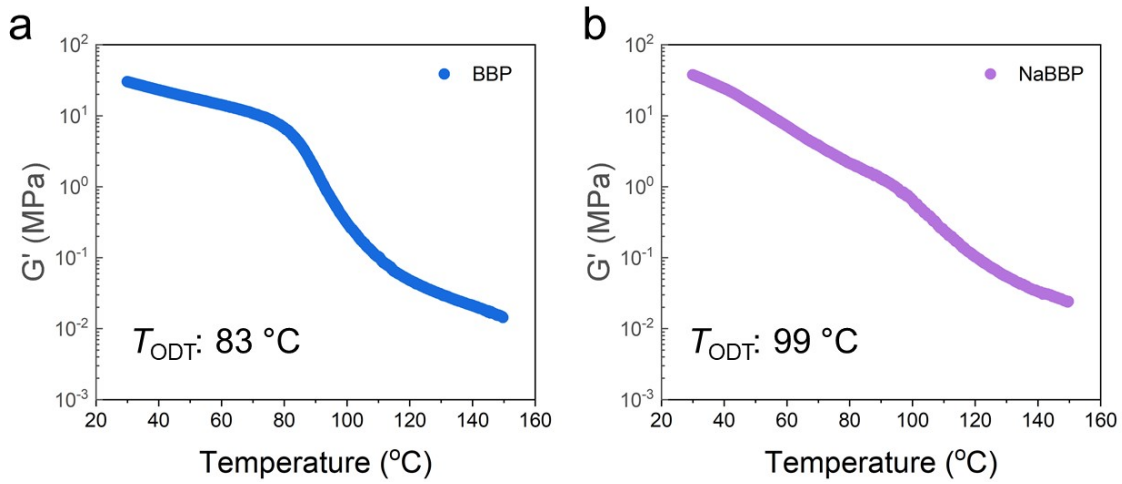

Fig. S7. Temperature-dependent storage modulus (G') of a) BBP and b) NaBBP (scan rate: 1 °C min^{-1}).

The order-disorder transition temperatures (T_{ODT}) of BBP and NaBBP were determined to be 83 and 99 °C, respectively, identified as the point where the storage modulus (G') drops during the temperature sweep from 30 to 150 °C at 1 °C min^{-1}. The existence of T_{ODT} strongly supports the phase separation of BBP and NaBBP.

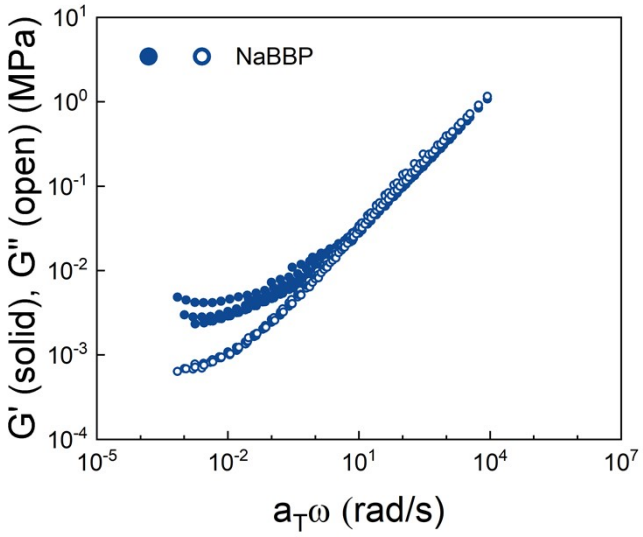

Fig. S8. TTS master curve of NaBBP.

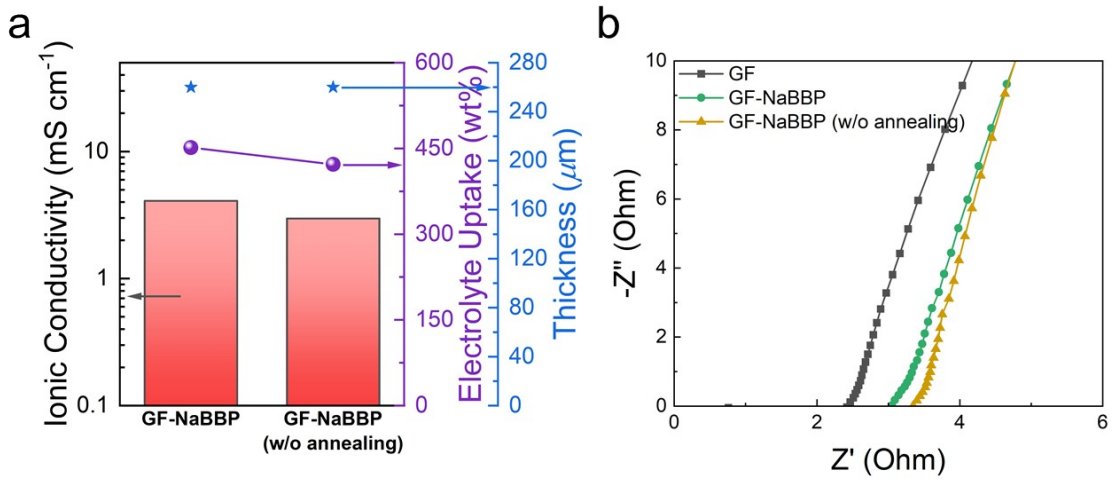

Fig. S9. a) Ionic conductivities, electrolyte uptakes, and thicknesses of GF-NaBBP and GF-NaBBP without annealing. b) Nyquist plot of GF, GF-NaBBP, and GF-NaBBP without annealing (test temperature: 30 °C).

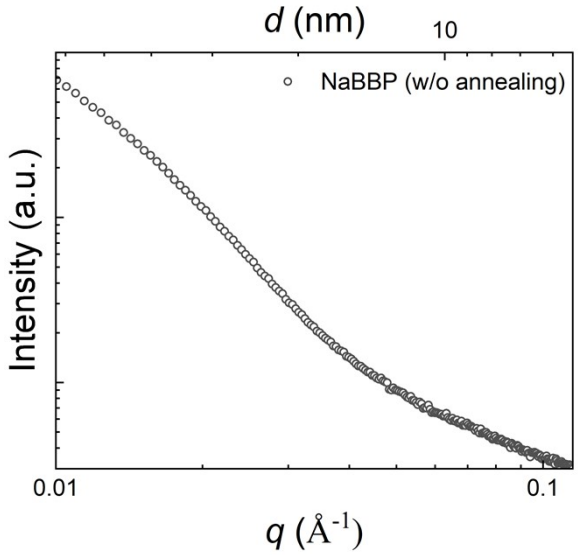

Fig. S10. SAXS profile of non-annealed NaBBP.

The absence of any scattering peak in the SAXS profile of the non-annealed NaBBP indicates its disordered state.

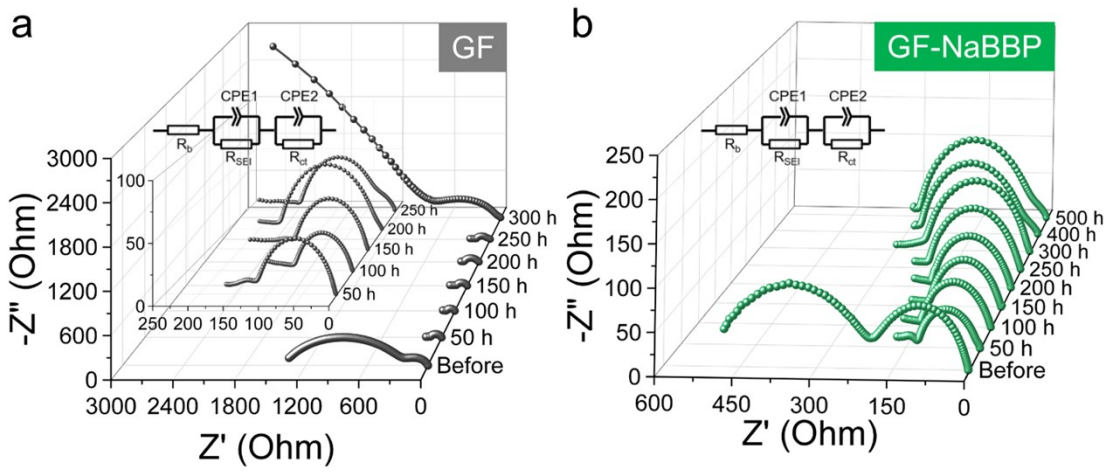

Fig. S11. Time-dependent electrochemical impedance spectra of symmetric Na/Na cells with a) GF and b) GF-NaBBP (test temperature: 30 °C).

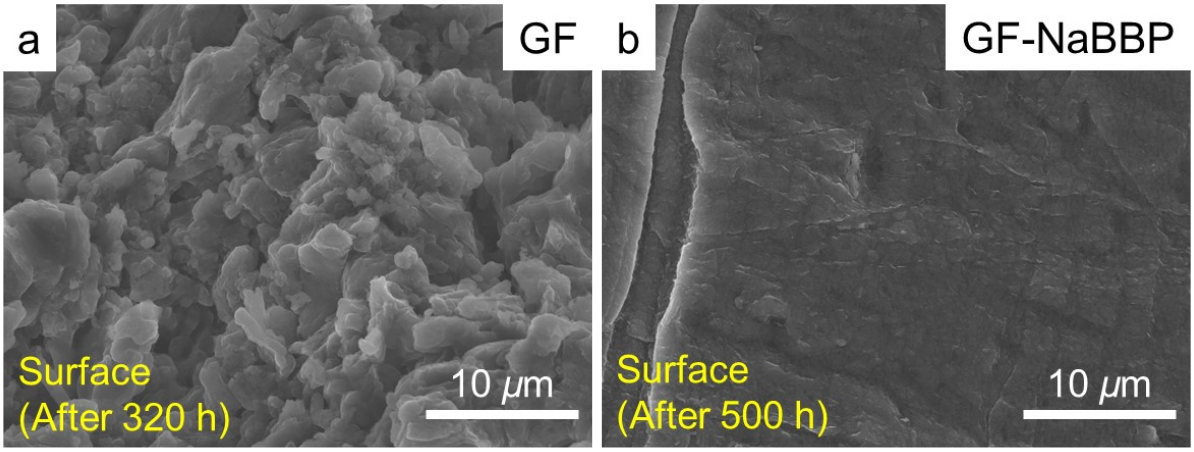

Fig. S12. Surface SEM images of Na metal from the symmetric Na/Na cells with a) GF and b) GF-NaBBP after galvanostatic cycling test.

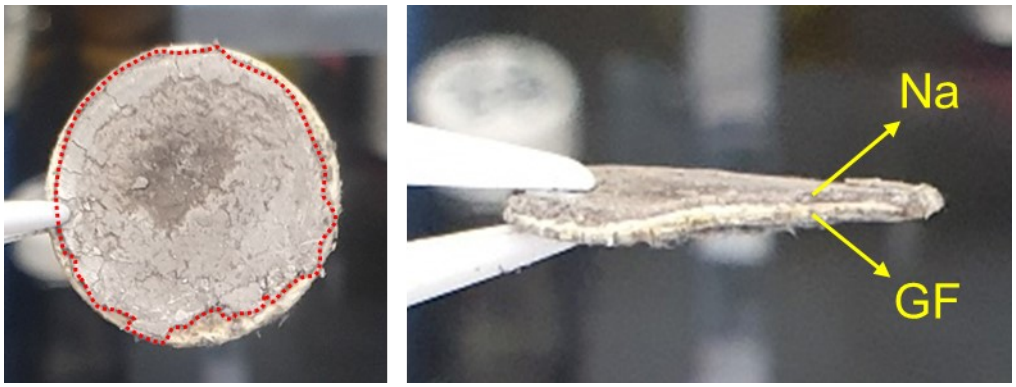

Fig. S13. Optical photographs of the cycled GF in the Na/Na symmetric cell for 200 h.

The inner region demarcated by the red-dashed line indicates Na metal attached to GF.

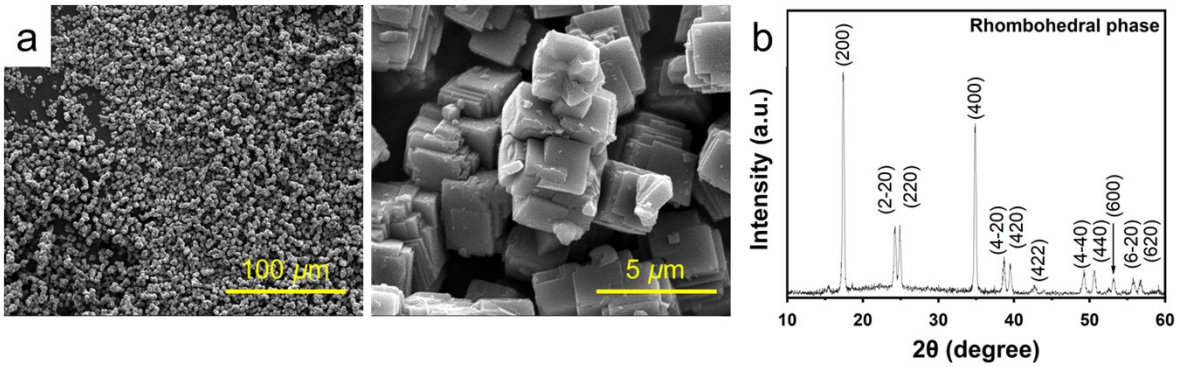

Fig. S14. a) SEM images and b) XRD pattern of PBA.

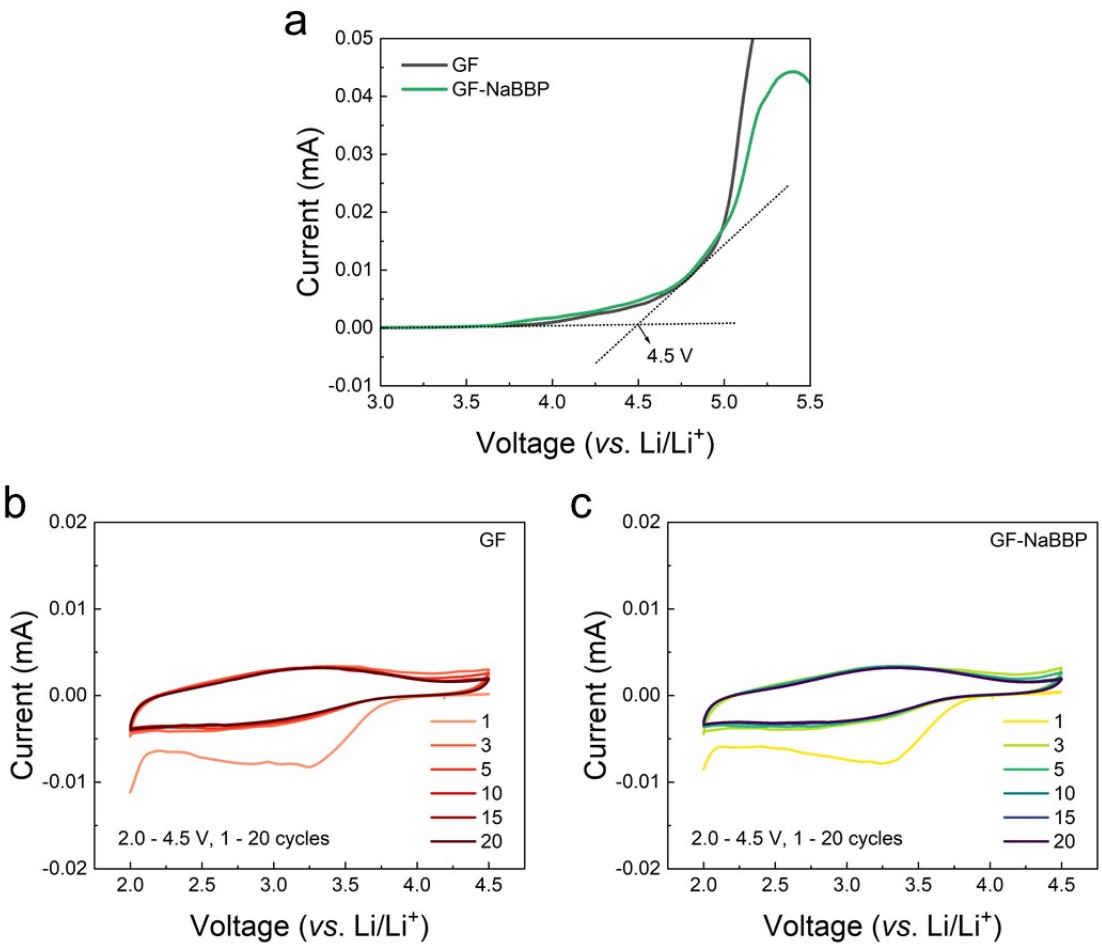

Fig. S15. a) LSV profiles of GF and GF-NaBBP. Cyclic voltammograms of b) GF and c) GF-NaBBP (scan rate: 1 mV s^{-1}, test temperature: 30 °C).

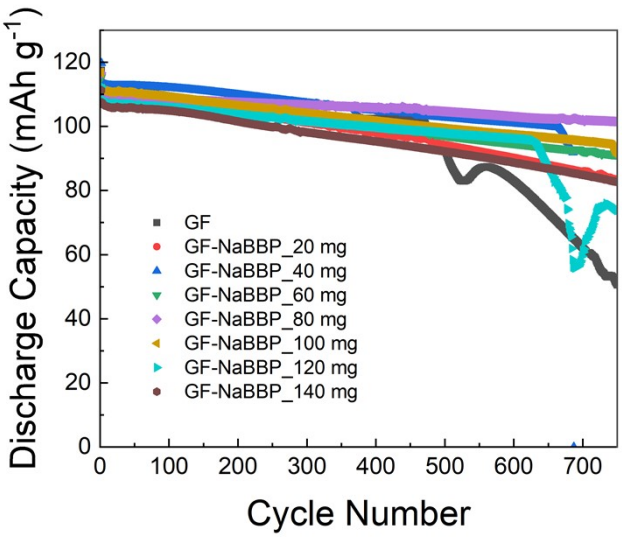

Fig. S16. Long-term cycling performance of Na/PBA cells with a series of GF-NaBBP prepared with varying NaBBP contents.

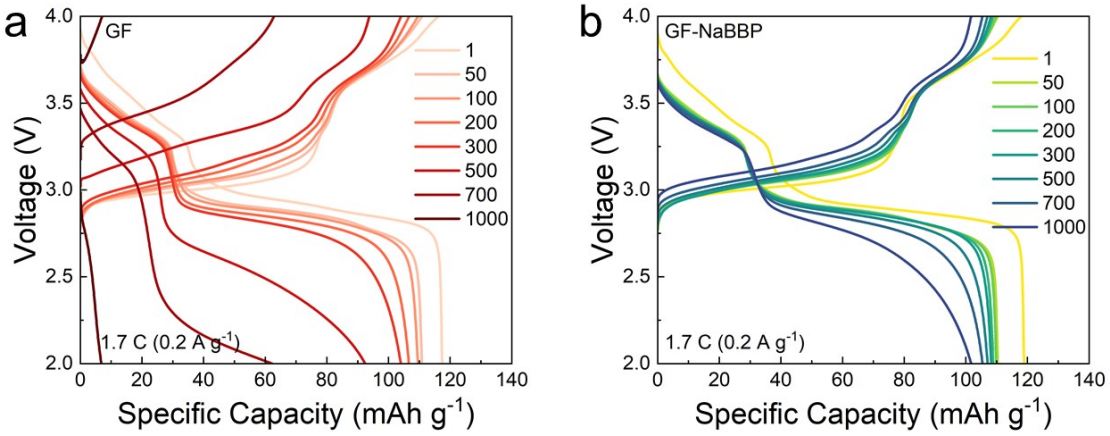

Fig. S17. Voltage-capacity profiles of the a) GF and b) GF-NaBBP cells cycled at 1.7 C (0.2 A g^{-1}). The legend indicates the cycle number of the corresponding charge/discharge curves.

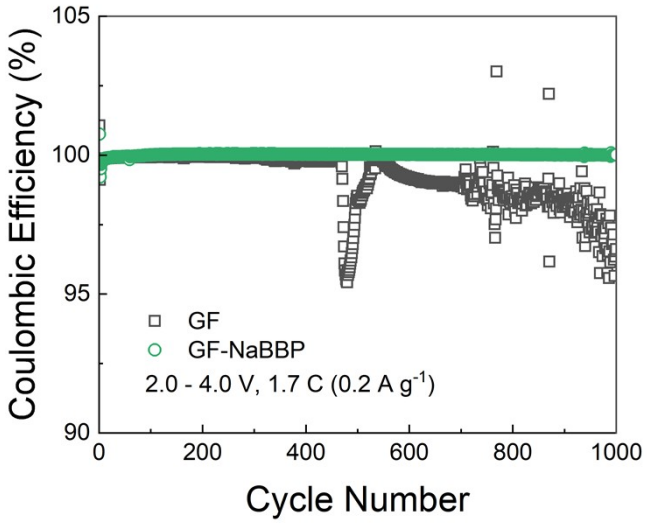

Fig. S18. Coulombic efficiency of the GF and GF-NaBBP cells during the long-term cycling tests at 1.7 C (0.2 A g^{-1}).

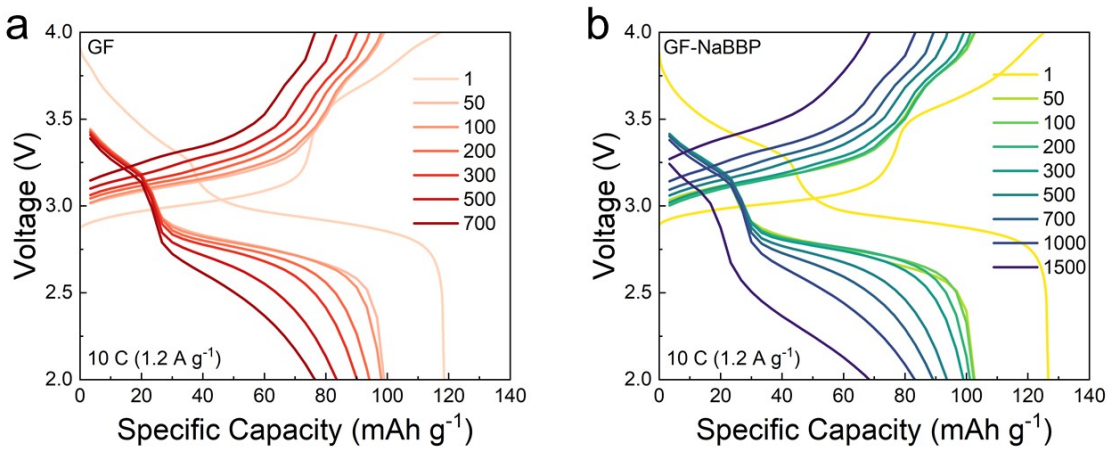

Fig. S19. Voltage-capacity profiles of the a) GF and b) GF-NaBBP cells cycled at 10 C (1.2 A g^{-1}). The legend indicates the cycle number of the corresponding charge/discharge curves.

Table S2. Comparison of cycle number, C-rate, and capacity retention values of the GF-NaBBP cell with previously published works.

Separator[a]	Cathode materials[b]	Cycle number	C-rate	Capacity retention (%)	Ref.
GF-NaBBP	PBA	1000	1.7	90	This work
		1500	10	65	
Perfluorinated sulfonic resin Na-form	PBA	1100	1	84.6	[6]
Poly(DOL)	PBA	1000	0.5	87.8	[7]
PVDF-HFP+ANs	NVP	1000	1	95.7	[8]
bis(trifluoroacetamide) SEI	PBA	500	1	86	[9]
Polyethersulfone+PVDF-HFP	NVP	500	1	97	[10]
PVDF-HFP+Cellulose acetate+NaTFSI+PC	NMNO	400	1	62	[11]
PTFE coated GF	NVPF	350	1	52	[12]
PP fiber interlayer	PBA	250	0.7	75	[13]
PVDF-HFP+IL+Polydopamine	PBA	100	0.2	94.7	[14]
Poly(trimethylene carbonate)+NaFSI	PBA	80	0.2	91	[15]

[a]Abbreviations for components; poly(1,3-dioxolane) (poly(DOL)), poly(vinylidene fluoride-*co*-hexafluoropropylene) (PVDF-HFP), Al_2O_3 nanowires (ANs), solid-electrolyte interphase (SEI), sodium trifluoromethanesulfonate (NaTFSI), propylene carbonate (PC), polytetrafluoroethylene (PTFE), polypropylene (PP), ionic liquid (IL), and sodium bis(fluorosulfonyl)imide (NaFSI). [b]Abbreviations for cathode active materials; $Na_3V_2(PO_4)_3$ (NVP), $Na_{0.67}Mn_{2/3}Ni_{1/3}O_2$ (NMNO), and $Na_3V_2(PO_4)_2F_3$ (NVPF).

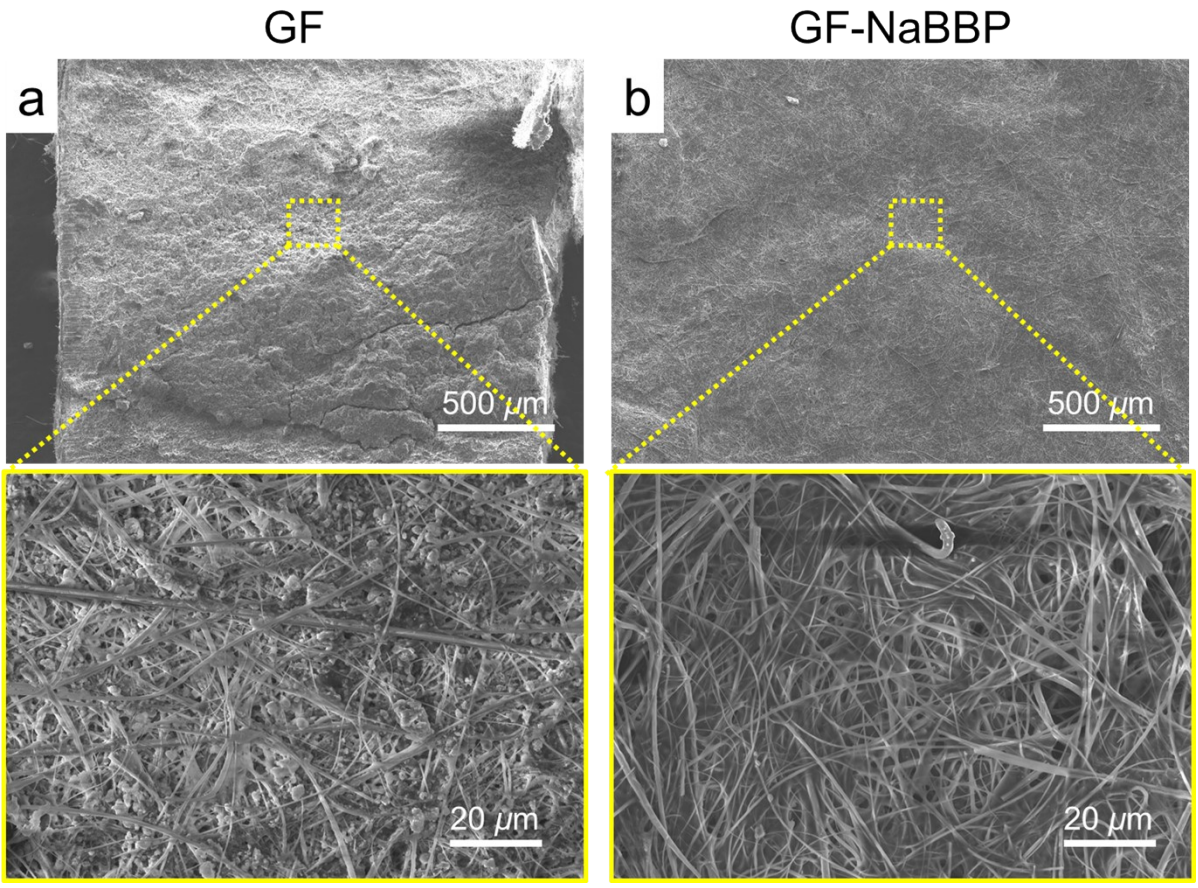

Fig. S20. Surface SEM images of (a) GF and (b) GF-NaBBP after 1000 cycles under 1.7 C.

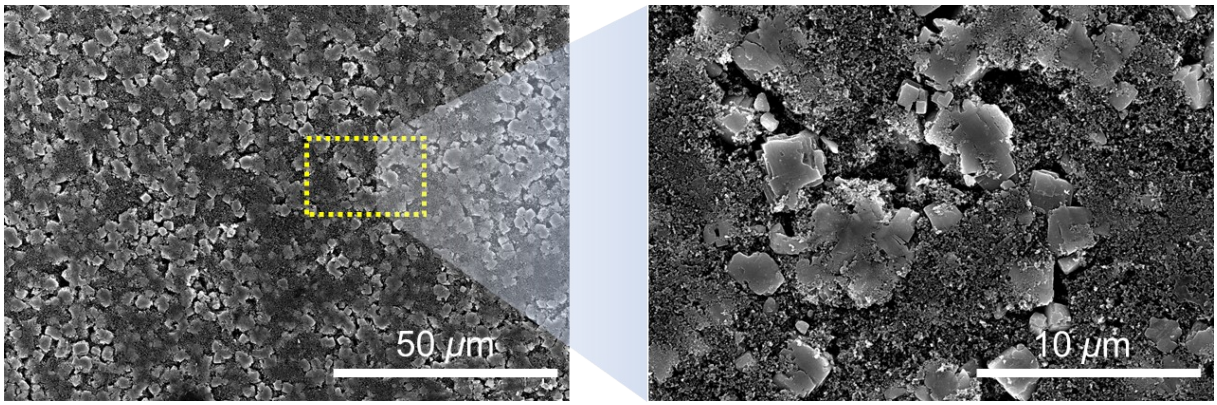

Fig. S21. Surface SEM images of the pristine PBA cathode.

The large cube-shaped particles are PBA (side length ≈ 2 μm) and the small sphere-shaped particles are super P (diameter ≈ 40 nm).

References

1. D. Jeong, D. S. Kwon, H. J. Kim and J. Shim, *Adv. Energy Mater.*, 2023, **13**, 2302845.
2. W. Wang, Y. Gang, Z. Hu, Z. Yan, W. Li, Y. Li, Q. F. Gu, Z. Wang, S. L. Chou, H. K. Liu and S. X. Dou, *Nat. Commun.*, 2020, **11**, 980.
3. H. Sun, *J. Phys. Chem. B*, 1998, **102**, 7338-7364.
4. P. P. Ewald, *Ann. Phys.*, 2006, **369**, 253-287.
5. B. A. Fortuin, J. Otegi, J. M. Lopez Del Amo, S. R. Pena, L. Meabe, H. Manzano, M. Martinez-Ibanez and J. Carrasco, *Phys. Chem. Chem. Phys.*, 2023, **25**, 25038-25054.
6. G. Du, M. Tao, J. Li, T. Yang, W. Gao, J. Deng, Y. Qi, S. J. Bao and M. Xu, *Adv. Energy Mater.*, 2019, **10**, 1903351.
7. Y. Shuai, J. Lou, X. Pei, C. Su, X. Ye, L. Zhang, Y. Wang, Z. Xu, P. Gao, S. He, Z. Wang and K. Chen, *ACS Appl. Mater. Interfaces*, 2022, **14**, 45382-45391.
8. D. Lei, Y. B. He, H. Huang, Y. Yuan, G. Zhong, Q. Zhao, X. Hao, D. Zhang, C. Lai, S. Zhang, J. Ma, Y. Wei, Q. Yu, W. Lv, Y. Yu, B. Li, Q. H. Yang, Y. Yang, J. Lu and F. Kang, *Nat. Commun.*, 2019, **10**, 4244.
9. C. Wang, Z. Sun, L. Liu, H. Ni, Q. Hou, J. Fan, R. Yuan, M. Zheng and Q. Dong, *Energy Environ. Sci.*, 2023, **16**, 3098-3109.
10. X. Li, J. Zhang, X. Guo, C. Peng, K. Song, Z. Zhang, L. Ding, C. Liu, W. Chen and S. Dou, *Adv Mater*, 2023, **35**, e2203547.
11. J. Pan, Y. Zhang, F. Sun, M. Osenberg, A. Hilger, I. Manke, R. Cao, S. X. Dou and H. J. Fan, *Angew. Chem. Int. Ed. Engl.*, 2023, **62**, 202219000.
12. H. Liu, X. Zheng, Y. Du, M. C. Borras, K. Wu, K. Konstantinov, W. K. Pang, S. Chou, H. Liu, S. Dou and C. Wu, *Adv. Mater.*, 2024, **36**, 2307645.
13. C. B. Soni, Sungjemmenla, S. K. Vineeth, C. S. Kumar and V. Kumar, *Sustain. Energy & Fuels*, 2023, **7**, 1908-1915.
14. M. Xie, S. Li, Y. Huang, Z. Wang, Y. Jiang, M. Wang, F. Wu and R. Chen, *ChemElectroChem*, 2019, **6**, 2423-2429.
15. C. Sångeland, R. Mogensen, D. Brandell and J. Mindemark, *ACS Appl. Polym. Mater.*, 2019, **1**, 825-832.